

Liang Wang · Daniel Fine · Deepak Sharma ·  
Luisa Torsi · Ananth Dodabalapur

## Nanoscale organic and polymeric field-effect transistors as chemical sensors

Received: 1 September 2005 / Revised: 26 September 2005 / Accepted: 28 September 2005 / Published online: 29 November 2005  
© Springer-Verlag 2005

**Abstract** This article reviews recently published work concerning improved understanding of, and advancements in, organic and polymer semiconductor vapor-phase chemical sensing. Thin-film transistor sensors ranging in size from hundreds of microns down to a few nanometers are discussed, with comparisons made of sensing responses recorded at these different channel-length scales. The vapor-sensing behavior of nanoscale organic transistors is different from that of large-scale devices, because electrical transport in a nanoscale organic thin-film transistor depends on its morphological structure and interface properties (for example injection barrier) which could be modulated by delivery of analyte. Materials used in nanoscale devices, for example nanoparticles, nanotubes, and nanowires, are also briefly summarized in an attempt to introduce other relevant nano-transducers.

### Introduction

Sensors with the ability to detect chemicals, for example volatile organic compounds (VOC), and biological species, including DNA and proteins, have been given increasing attention by the scientific and industrial communities. This is because of their great potential in an array of applications in manufacturing, transportation, environmental monitoring, process control, drug delivery, homeland security, and national defense [1–5]. Most currently available commercial products are, however, bulky, costly, and require long

time periods for sampling and for analyzing data. A novel scheme which employs portable inexpensive devices, with the advantage of rapid retrieval, is desired. Miniaturization is demanded for all types of sensor, because of the need for better portability, higher sensitivity, lower power dissipation, and better device integration [6, 7]. Many types of sensor have been evaluated for this purpose. A variety of transduction techniques have been used, for example acoustic wave devices [8, 9], electrochemical resistive sensors [10, 11] and field-effect transistors with a chemical sensing gate (CHEMFETs) [12, 13]. Among these sensing schemes, field-effect transistors have attracted increasing interest, because of their ability to amplify in-situ and to gate-modulate channel conductance, as well as their compatibility with well-developed microelectronic fabrication techniques which enable miniaturization.

The organic thin-film transistor (OTFT) is a promising sensor device for an electronic olfaction platform with all the required features (sensitivity, reliability, and reproducibility) at low cost. Compared with CHEMFETs or chemiresistor sensors, an OTFT sensor can provide more information from changes in multiple properties on exposure to an analyte, for example the bulk conductivity of an organic thin film, the field-induced conductivity, the transistor threshold voltage, and the field-effect mobility [14]. Organic and polymeric field-effect transistors employing different active layers can be used to detect a variety of analyte molecules with good stability and sensitivity [15]. Chemical detection is possible by use of direct semiconductor–analyte interactions, by use of specific receptor molecules, selective for the analytes, percolated throughout the semiconductor layer, by variation of the end/side groups of the semiconductor material, and by controlling the thin-film morphology of the semiconductor layer. These advantages of OTFT are a basis for construction of combinatorial arrays of sensors with different responses to the components of a mixture of odors. Gas-sensing complementary circuits and logic gates with OTFTs have also been demonstrated [16]. These advances, in addition to circuitry for pattern recognition, could lead to an electronic nose.

L. Wang · D. Fine · D. Sharma · A. Dodabalapur (✉)  
Microelectronics Research Center,  
The University of Texas at Austin,  
Austin, TX 78758, USA  
e-mail: ananth@mer.utexas.edu  
e-mail: frkwang@gmail.com

L. Torsi  
Dipartimento di Chimica, Università degli Studi di Bari,  
4 via Orabona,  
70126 Bari, Italy  
e-mail: torsi@chimica.uniba.it

For any analyte, use of nanoscale-dimension devices in organic transistor sensors results in very different sensor mechanisms compared with micron-sized devices with the same semiconductor. This is because in a large-scale device (channel length much larger than the active layer grain size) the sensing mechanism is analyte-mediated charge trapping, which usually leads to a decrease in device current on exposure to the analyte. In nanoscale devices the analyte molecules modulate the charge carrier injection at the source and drain electrodes. This can lead to large increases in device current which implies that such sensors are more sensitive. It is known that electrical transport in very short channel-length organic transistors is contact-limited and we believe that the analyte molecules diffuse near the source/drain contacts through the porous semiconductor layer. The analyte molecules can affect the behavior of the contact [17]. The smaller the channel length, the stronger this effect is. As shown by the experimental evidence discussed later in this review, the behavior of nanoscale OTFT sensors is remarkably different from that of their micro-scale counterparts. For OTFTs of such small dimensions the drain current typically increases by a factor  $>5$  in response to the analyte ( $>10$  for some devices). This provides a strong argument for employing nanoscale channel-length devices for sensing.

#### Organic field-effect transistors for sensing applications

This review will first introduce polycrystalline organic and polymeric thin-film field-effect transistors and then cover such topics as the proper detection of sensing signals from nanoscale device configurations, the dependence of sensing behavior on the geometry of device and material, and the sensing mechanisms in these sensors. We will also address several aspects of the interactions which produce sensing effects in electronic devices, and the trend toward better device performances and further commercialization. Finally other emerging nanoscale sensors will also be summarized, for example nanocrystal, carbon nanotube, and nanowire sensors for electrical detection of biological events.

Since the milestone discovery of conducting polymers in 1977 [18], much work has been done with small organic molecules and conjugated polymers to manufacture devices which take advantage of the unique properties of their conjugated  $\pi$ -electron systems. These include organic light-emitting diodes (OLEDs), solar cells, smart cards, resistive chemical sensors, and field-effect transistors [19–22]. Among these applications, the structure of field-effect transistors, with the organic or polymer semiconductor as the electrically active layer, enables study of the two-dimensional transport properties of the semiconductor material modulated by the charge carrier density because of increased gate bias [23–25]. An upside-down transistor structure (see Figs. 1 and 2 for an example) has been commonly used in organic FETs comprising rigid or flexible substrates, usually a highly doped silicon wafer or a metal-covered plastic sheet, followed by a dielectric

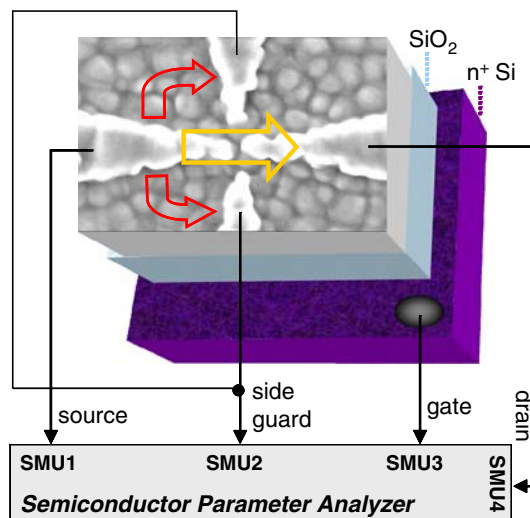


**Fig. 1** Three-dimensional device structure, and circuit diagram, for use of side guards in the measurements of a nanoscale transistor used as a chemical sensor. To collect spreading currents traveling through the area outside the defined channel, two side guards were designed on the two sides of the channel, unconnected to and kept at the same potential as the drain. The three layers, from the top, are bottom-contact pentacene and Au/Ti electrodes (surface shown by an SEM image of a real device), SiO<sub>2</sub> as dielectric, n<sup>+</sup> Si as gate. Each SMU (source-measurement unit) of the semiconductor parameter analyzer (Agilent 4155C) supplies voltage and measures current independently. SMU1, 2, 3, and 4 serve as the source, side-guard, gate, and drain, respectively. SMU1=ground; SMU3= $V_g$ ; SMU2 and SMU4 were set at the same value  $V_{ds}$ .

layer, for example silicon dioxide or an insulating polymer. The organic or polymer semiconductor and metallic source and drain contacts are then deposited on top of the gate dielectric [26–28]. This kind of structure reduces fabrication complexity and enables direct access to the active semiconducting layer to investigate its structure and morphology and how they relate to the device's electrical properties. Field-effect transistors with high mobilities have been made from small organic molecules, such as pentacene, and have been deposited by sublimation [29, 30]. Soluble conjugated polymers, for example regio-

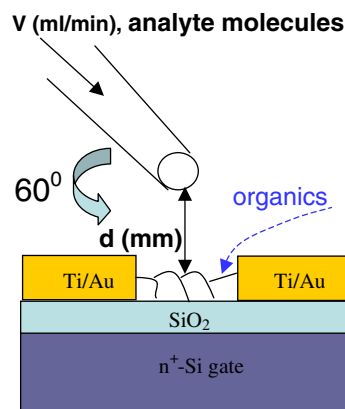


**Fig. 2** The schematic structure of a bottom-contact organic thin-film transistor. Its organic semiconductor channel, which serves as the sensing layer, is exposed to the analyte vapor delivered with a controlled flux through a carefully positioned syringe

regular polythiophene, have been deposited by spin-coating, solution-casting, or ink-jet printing processes [31–33]. Chemical sensors made from organic or conjugated polymeric transistors are operated at room temperature, an advantage compared with inorganic Metal Oxide Semiconductor Field Effect Transistor (MOSFET) sensors. Upside-down organic thin-film transistor (TFT) sensors use the organic semiconductor active layer as the transducer; this interacts with airborne chemical species referred to as analytes. This interaction directly affects the conductive channel, unlike sensors made of inorganic MOSFETs [34–37] or insulated gate FETs (IGFETs use the polymer layer as the gate for a silicon FET [6]) in which the sensing events occur at the gate or gate/insulator boundary and indirectly modulate the current by capacitive coupling. This means conductivity in the upside-down structure can be effected by changes in mobility (and by changes in charge density) which is not possible in the other sensor configurations. These upside-down organic and polymer sensors can be refreshed by reverse biasing the gate (a high positive voltage for a p-channel, a high negative voltage for an n-channel) to remove the trapped charges which result from the semiconductor–analyte interaction.

There have been reports of investigation of the chemical sensing effects of organic and conjugated polymer transistors [15, 16, 38–40]. It has been shown that on large-scale devices ( $L > 1 \mu\text{m}$ ), alkyl chain alcohol analytes interact with polythiophene thin-films at grain boundaries and at the dielectric interface rather than the bulk of the film [41]. There have recently been reports on the role of the side-chain in chemical sensing of polymer/oligomer based field-effect transistors [40, 42]. Other articles have reported sensing effects dependent on the channel length to grain size relationship in large-scale organic transistors [43, 44]. There is also an increasing need to develop sensors with very small active areas, not only to reduce power requirement, but also for higher sensitivity [45]. According to our experimental findings and analysis, however, the effect of scaling down the geometry of an organic field-effect transistor (OFET) device is not merely as simple as enhancing the sensitivity. Instead, the sensing mechanism of where and how analyte molecules affect electrical transport in an organic transistor might be quite different for nanoscale-dimension devices. The main reason is that, unlike the MOSFET with crystalline silicon channel, the electrical transport and chemical sensing behavior of a polycrystalline OFET depend heavily on the morphological structure of the channel material and the properties of interfaces. For large-scale OFET devices, grain boundaries play the dominant role in both electrical transport and chemical sensing behavior. For smaller channel length, the number of grain boundaries within a channel decreases so that the amount of effect of grain boundaries on electrical transport and chemical sensing reduces and other factors become more important. At smaller channel dimensions, especially when the channel length is comparable with or smaller than the grain size of polycrystalline organic molecules or conjugated poly-

mers, we might possibly observe the electrical transport and chemical sensing behavior within the body of grains; the mechanism of this might be different from that in large-scale devices in which grain boundaries dominate. The contact barrier at the interface between electrode and semiconductor will also play an important role when scaling down, because resistance through the semiconductor channel is smaller. We believe it is the injection of current at the source/drain contacts that is modulated by the analyte molecules [17]. Thus the behavior of nanoscale OFET sensors is markedly different from that of larger channel-length devices.

Previous work on micro-sized OTFT vapor sensing and its correlation with thin film morphology

The vapor sensing behavior of nanoscale organic transistors is different from that of large-scale devices, because electrical transport in an OTFT depends on its morphological structure and interface properties and analyte molecules are able to interact with different parts of a device and modulate its conductance. In previous work on micro-sized OTFTs made of a variety of active semiconductor layers [15, 43], Crone and Torsi et al. investigated the relationship of vapor sensing to thin-film morphology on exposure to different analyte molecules. Correlation of the vapor response characteristics to the length of end groups (flexibility at the molecular level) and grain size (porosity at the morphological level) of the semiconductor was demonstrated by observing the transient source-drain current under vapor flow and performing transmission electron microscopy (TEM) for morphological characterization.

These experiments demonstrated that the sensing response of OTFT channels to analytes with moderate dipole moments (e.g. alcohols) is enhanced with decreased grain size and looser molecular packing of the organic semiconductor layer. Smaller grains yield more grain boundaries which increases interaction sites. The response also increases with increasing film thickness, again because of the increased number of grain boundaries (the surface morphology becomes more structured as the films grow thicker from the flat and featureless ultra-thin film). Analytes binding to the disordered and thinner grain boundaries are closer to the channel than those on the top surfaces of the grains and thus exert greater influence on the conductivity.

It was also found that the sensing response increased as the length of the organic semiconductor's hydrocarbon end group increased. This is because of the elongated lamellar morphology and looser molecular packing, which enable greater access of analyte vapor and increased surface area and change the electronic or spatial barriers between grains. The alkyl chains therefore facilitate adsorption of the analyte molecules by the sensing film. This adsorption mechanism could be a combination of hydrophobic interactions, intercalation to fill defect vacancies, and simple surface binding. All these processes are favored at grain boundaries.

The interaction between organic semiconductor and analyte molecules is still not yet completely understood. The adsorbed polar analyte could affect charge transport in the channel by trapping some charges and consequently reduce the mobility of other mobile charges in the channel. The main effect of the trapped or otherwise immobile charges at the dielectric interface is, however, to induce a threshold shift in the transistor characteristics. For alcohol sensing, a constant threshold shift was observed at low gate voltages which became a gate voltage-dependent mobility change at high gate voltages. It was also observed that a reverse gate bias can facilitate restoration of the drain current to near its original value.

The interaction between the alcohol and the organic film of the OTFT does not involve the bulk of the crystalline grains of the film, because no change in refractive index and thickness was observed with a single wavelength ellipsometer during the exposure of the film to the analyte vapor. It was suggested that the sensing interaction is a surface-type interaction involving grain boundaries.

#### The design of guarding electrodes for true detection of nanoscale sensor activity

Nanoscale organic field-effect transistors have been fabricated by several groups [47–49]. It is, however, technically difficult to pattern the active semiconductor area of devices with such small channel lengths. For transistors with a channel length near and below 10 nm, a large  $W/L$  ratio is not favorable, because of a higher chance of shorted electrodes [49] and electrode edge roughness of the order of the channel length. Consequently, the spreading currents which travel outside the defined channel cannot be ignored for devices with small  $W/L$  ratios. We designed a separated pair of guard electrodes at the two sides of the channel, unconnected to and kept at the same potential as the drain. These guarding electrodes collect the spreading currents so that the drain current measured, the direct current from source to drain [50], excludes contributions from macroscale spreading currents, as shown in Fig. 1. Devices were fabricated where the channel length is below 50 nm, with a small  $W/L$  ratio, and in which the active semiconductor layer and gate are not patterned. The distance between a channel and its side guards in the devices produced ranges from 20 nm to 50 nm, comparable with the channel lengths. Measurements of the drain current were taken on the same device with ( $I_{ds}$ ) and without ( $I_{open}$ ) biasing the side guards. For nanoscale devices,  $I_{ds}$  and  $I_{open}$  resulted in different behavior. Use of  $I_{open}$  resulted in behavior more like that of a long-channel FET, probably because of a substantial spreading current component. This novel four-terminal geometry design provides a powerful capability to investigate the sensing behavior within the nanoscale active area through the defined channel without any undesirable background from large-scale parasitic parallel conduction pathways around the channel [50].

#### Justification and fabrication of organic and polymeric transistors

With the four terminal methodology we fabricated transistors with organic molecules (pentacene) and conjugated polymers (regioregular poly(3-hexylthiophene), P3HT) which included a range of channel lengths from a few hundred microns down to sub 10 nm. The field-effect characteristics of organic semiconductors as the channel layer, and their responses to analytes as the sensing layer, were characterized to systematically investigate the relationship between the sensing behavior and geometry factors of the channel. The grain size of the organic semiconductor was also varied to investigate the role of scale in organic transistor sensing behavior. Pentacene was chosen as the active layer, because of its relatively high mobility and wide use in organic electronics and sensors [51, 52]. P3HT is a soluble conjugated polymer with relatively high mobility and thus has a great potential to be manufactured into chemical sensors with low-cost techniques such as ink-jet printing [53–55]. The analytes we use to test nanoscale devices are 1-pentanol and vanillin. Various types of analyte have been used to investigate the chemical sensing responses of long-channel devices, and we have found 1-pentanol is a prototypical alcohol analyte for representing their sensing behavior. Vanillin is widely used in pharmaceuticals, perfumes, and flavors.

The transistor device structure (bottom-contact devices) is shown in Fig. 2. This device configuration enables the organic semiconductor to be operated simultaneously as both the transistor channel and the sensing layer on exposure to the analyte molecules. A heavily doped n-type silicon substrate serves as the gate. Transistors of channel length greater than 1  $\mu\text{m}$  use a 100 nm thermally grown  $\text{SiO}_2$  layer as the gate dielectric, whereas for nanoscale transistors, a 5 nm  $\text{SiO}_2$  layer as the gate dielectric was grown by rapid thermal annealing in oxygen. 3 nm Ti/45 nm Au was deposited by e-beam evaporation on to the wafer after e-beam lithography (for submicron channel lengths) or photolithography (for micron channel lengths). With lift-off, electrode patterns of channel lengths down to 15 nm were obtained. Sub 10 nm channels were created by electrophoresis trapping bridge and break junction techniques [56, 57]. Electrode patterns of channel lengths  $>100 \mu\text{m}$  were realized directly by metal evaporation through shadow masks. Pentacene (purchased from Aldrich), 300–600  $\text{\AA}$ , was thermally evaporated in a base vacuum of approximately  $3 \times 10^{-7}$  Torr at different growth rates and different substrate temperatures for different grain sizes. For channel lengths greater than a micron an elevated substrate temperature (80°C) and medium growth rate ( $1.9 \text{ \AA s}^{-1}$ ) during deposition resulted in large grains with an average size of 1  $\mu\text{m}$ . Nanoscale channels comprising larger pentacene grains, with an average size of 250 nm, were achieved by use of a slow growth rate ( $0.5 \text{ \AA s}^{-1}$ ) and room-temperature deposition. High growth rates (4.4–7.1  $\text{\AA s}^{-1}$ ) at room temperature during thermal evaporation

will give a pentacene layer of small grains with an average size of 80–140 nm. Regioregular P3HT was synthesized as described by Bao et al. [31]. The P3HT was dissolved in chloroform (approx. 0.1% by weight). Solutions were filtered through 0.2  $\mu\text{m}$  pore size PTFE membrane syringe filters. Bottom contact devices were completed by solution-casting with a custom ink-jet type deposition apparatus to inject the solution and limit the coverage area to within 200  $\mu\text{m}$  to reduce leakage through gate dielectric. Preparation of the devices was completed by immediate transfer into a vacuum oven to evaporate the solvent for 36 to 48 h.

### Characterization measurements and sensing experiments

The DC electrical characteristics of the transistors were measured with an Agilent 4155C semiconductor parameter analyzer. The transient variation of drain current  $I_{\text{ds}}$  was then examined under fixed gate ( $V_{\text{g}}$ ) and source–drain ( $V_{\text{ds}}$ ) potential in air at room temperature. A peristaltic pump was used to drive air through a transfer line (Tygon tube) into a monojet syringe to deliver the saturation vapor there to sensing devices. To provide the saturated analyte vapor, the syringe contained a piece of analyte-soaked filter paper and was fixed on to a three-dimensional micromanipulator to ensure proper alignment of the vapor outlet to the transistor channel. A solenoid valve was placed in the middle of the transfer line to switch the analyte delivery. The analyte flux ( $v$ ) and the syringe nozzle–device distance ( $d$ ) were varied to examine the effect of analyte delivery on the sensing responses. Currents were measured throughout the entire measurement period whereas the analyte was delivered for a certain duration only, to facilitate comparison of the drain current behavior before, during, and after exposure to the analyte.

Before every sensing measurement, each device was tested with pure air and no sensing effect on drain current was detected. The currents in the absence of analyte decrease continuously over time, because of bias stress effect. This is a well-known effect in organic field-effect transistors in which the current slowly decreases with time for a fixed bias, because the field-induced carriers (holes) fall into deep trap states where they are less mobile, which results in a reduction of current [58, 59]. The sensor response is superposed on this background, which can be reversed by using a reverse bias configuration (high positive gate voltage) to recover the device characteristics. The measured leakage currents through the gate dielectric were negligible compared with the drain currents. After the measurements, all the devices were examined by a field-emission SEM and no deterioration in morphology was found.

The mobilities of the pentacene transistors were of the order of  $10^{-2} \text{ cm}^2 \text{ V}^{-1} \text{ s}^{-1}$ , with a highest value of  $0.045 \text{ cm}^2 \text{ V}^{-1} \text{ s}^{-1}$  observed in air for the transistors with pentacene grain size of 1  $\mu\text{m}$  and channel length of 36  $\mu\text{m}$ . Figure 3 shows the characteristics of a 60 nm channel ( $W/L=10$ ) with pentacene grain size of 80 nm, measured in

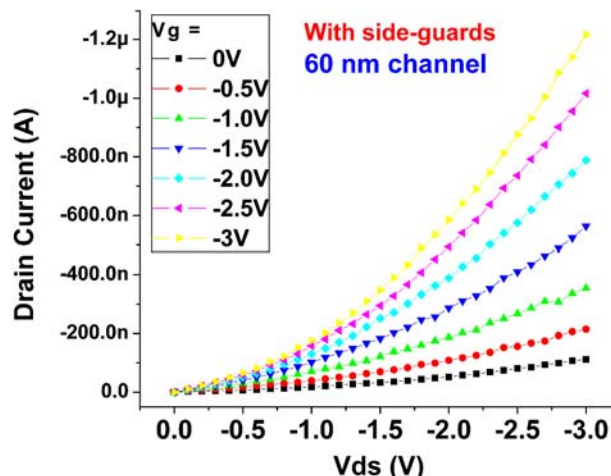


**Fig. 3** Characteristics of a pentacene transistor of 60 nm channel ( $W/L=10$ ) used for sensing measurements, measured in a vacuum of 2.4 mTorr, calculated mobility= $0.021 \text{ cm}^2 \text{ V}^{-1} \text{ s}^{-1}$ . Reprinted with permission from Liang Wang, Daniel Fine, and Ananth Dodabalapur, Applied Physics Letters, 85, 6386 (2004). Copyright 2004, American Institute of Physics

vacuum. Its mobility was calculated to be  $0.021 \text{ cm}^2 \text{ V}^{-1} \text{ s}^{-1}$ . The mobilities of most P3HT transistors measured in air at room temperature were approximately  $10^{-3} \text{ cm}^2 \text{ V}^{-1} \text{ s}^{-1}$  and only a small number of devices had a mobility approaching  $10^{-2} \text{ cm}^2 \text{ V}^{-1} \text{ s}^{-1}$ . Fig. 4 shows the characteristics of a P3HT transistor with a channel length of 125 nm and channel width of 275 nm, corresponding to a mobility of  $1.2 \times 10^{-2} \text{ cm}^2 \text{ V}^{-1} \text{ s}^{-1}$  in the linear region of operation. Despite the relatively high off-current, these plots are indicative of reasonable gate modulation. The super-linear feature of these devices is because of the contact barrier between the conjugated polymer and the gold electrodes. In devices in which the mobility of the organic semiconductors is relatively high, the contact barrier becomes the

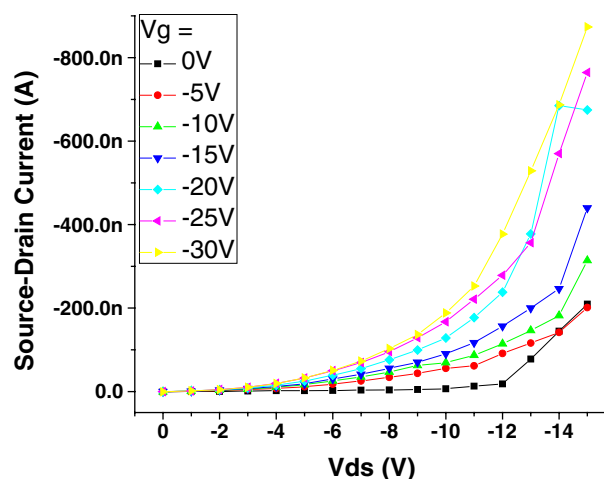


**Fig. 4** The DC characteristics of a 125 nm channel ( $W=275 \text{ nm}$ ) P3HT transistor in air at room temperature. The mobility is  $1.2 \times 10^{-2} \text{ cm}^2 \text{ V}^{-1} \text{ s}^{-1}$  in the linear region of operation. Reprinted from Sens Actuators B (in press), Liang Wang, Daniel Fine, Saiful I Khondaker, Taeho Jung, Ananth Dodabalapur, Sub 10 nm conjugated polymer transistors for chemical sensing, Copyright (2005), with permission from Elsevier

bottleneck of transport which can be seen as the super-linear feature in the characteristics. The distribution of mobilities from device to device may be because of the difference in the semiconductor's local order.

#### *The function of guarding electrodes in chemical sensing*

A transistor with a 7 nm channel was made by trapping bridge and break junction technique [55, 56]. To investigate the sensing response from the sensor-active area in truly nanoscale geometry and the role of the side-guarding electrodes in sensing measurement, we recorded the drain current transients on exposure to 1-pentanol without and with use of side-guarding function, as shown in Figs. 5(a) and 5(b) respectively. Surprisingly, Fig. 5(a) and 5(b) are indicative of opposite sensing response directions. Without the side guarding function, the transient shown in Fig. 5(a) represents the sensing behavior of the large area around the channel, which is a decrease in drain current by 20–25%. With the side guarding function to eliminate most of the spreading current (two side guarding electrodes biased at the same potential as the drain), the transient in the drain current [Fig. 5(b)] represents the true sensing behavior of the nanoscale active area, which is an increase in drain current of approximately a factor of 2. Fig. 5(c) shows the variation of the side current (collected at side guarding electrodes) corresponding to that of the drain current [Fig. 5(b)], which was measured simultaneously with Fig. 5(c). The side current response to the analyte is markedly different from the drain current in Fig. 5(b)—the side current shows a decrease in response to the analyte whereas the drain current simultaneously shows an increase on exposure to the analyte. Because Fig. 5(b) and 5(c) were recorded simultaneously and showed different kinds of sensing behavior, it is evident that the side current is the spreading current traveling outside the defined channel excluding the direct current through the nanoscale channel which is collected at the drain simultaneously. Therefore, by utilizing the side guarding function we can eliminate most of the contribution from the spreading current and detect the true sensing response of a nanoscale channel. The experimental findings obtained with this unique side-guard function are presented below for chemical sensing responses dependent on scaling geometry, analyte delivery, gate modulation, and different types of analyte.

#### *Scaling behavior of sensing responses*

We investigated the response of  $I_{ds}$  (operated in saturation region) on exposure to saturated vapor of 1-pentanol, with a series of channel length and varied grain sizes of pentacene under the same experimental conditions. As shown in Fig. 6(a), whereas a decrease in current was observed for the long channel-length devices on delivery of the analyte, an increase, sometimes by a factor  $>5$ , was

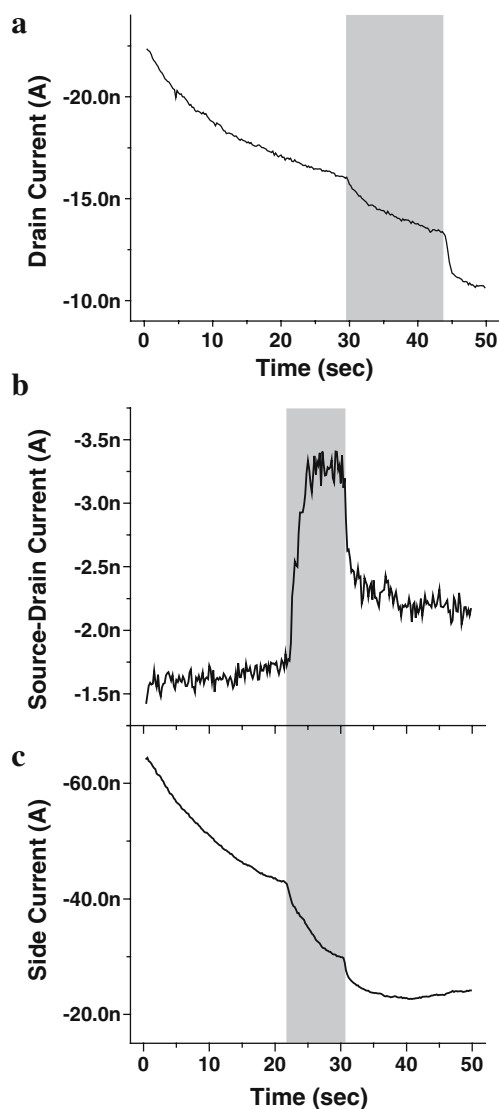


**Fig. 5** The sensing effects of 7 nm channel P3HT transistors on exposure to saturated 1-pentanol vapor. (a) The sensing response at  $V_g = -20$  V and  $V_{ds} = -1.5$  V, without applying side guarding electrodes. (b) and (c) are the sensing responses of currents simultaneously collected at the drain and side electrodes respectively, with side guarding electrodes at the same potential as the drain to collect spreading current, at  $V_g = -20$  V and  $V_{ds} = V_{side} = -1.5$  V. Reprinted from Sens Actuators B (in press), Liang Wang, Daniel Fine, Saiful I Khondaker, Taeho Jung, Ananth Dodabalapur, Sub 10 nm conjugated polymer transistors for chemical sensing, Copyright (2005), with permission from Elsevier

observed for the small channel-length devices. Two mechanisms influence sensor behavior: one causing a decrease in current (dominant in large  $L$  devices) and the other causing an increase (dominant in small  $L$  devices). The crossover of response behavior depends on grain size, occurring in the interval of channel length between 150–450 nm for  $\sim 80$  nm grain size. Under the same conditions, when the average grain size of pentacene is increased to 250 nm, crossover behavior is observed for the sensors at larger channel lengths (from 450 nm to 1  $\mu\text{m}$ ), as shown in Fig. 6(b). Figure 6(c) shows the SEM image (after mea-

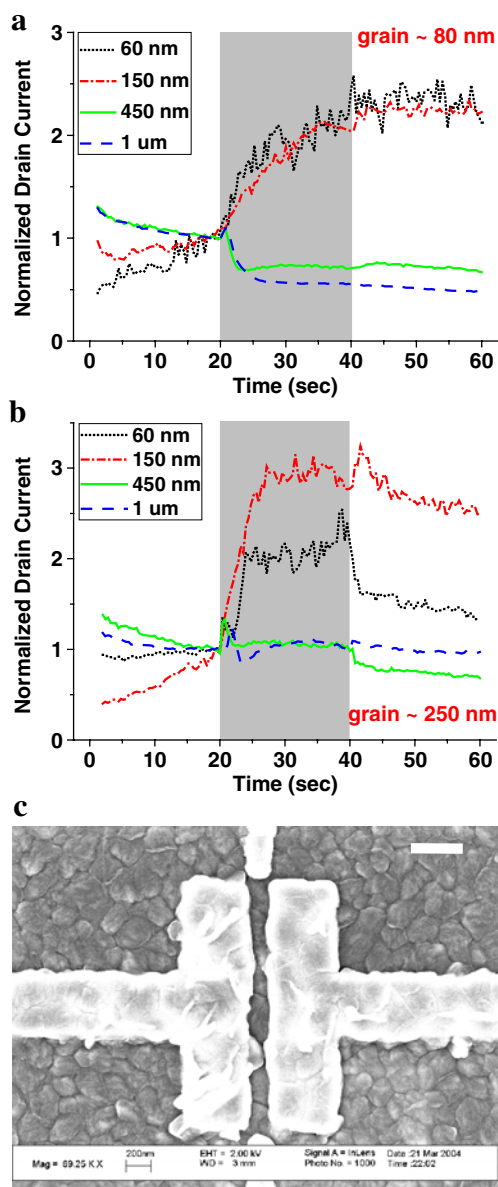


**Fig. 6** The sensing effects of pentacene transistors on exposure to 1-pentanol. **(a)** Sensing data of  $I_{ds}$  (normalized to that measured just before the analyte took effect) for 80 nm pentacene grain size and different nanoscale channel lengths (same  $W/L=10$ ), measured at  $V_g=V_{ds}=V_{side}=-2.5$  V (two side guards were kept at the same potential as the drain),  $v$  (analyte flux)=45 mL min<sup>-1</sup>,  $d$  (distance from syringe nozzle to device)=2 mm. **(b)** Sensing data of normalized  $I_{ds}$  for 250 nm pentacene grain size, measured at the same conditions as **(a)**. **(c)** SEM image taken after sensing measurements of a 150 nm channel with an average pentacene grain size of 250 nm, scale bar=400 nm. The grains appearing in the figure are pentacene. Reprinted with permission from Liang Wang, Daniel Fine, and Ananth Dodabalapur, Applied Physics Letters, 85, 6386 (2004). Copyright 2004, American Institute of Physics

surements) for a 150 nm channel which is smaller than the covering pentacene grains (~250 nm).

Figures 7(a) and 7(b) show the sensing responses of long-channel devices with pentacene grain size of 140 nm and 1 μm respectively. For all devices with channel lengths of 2 μm or greater,  $I_{ds}$  resulted in decreasing responses

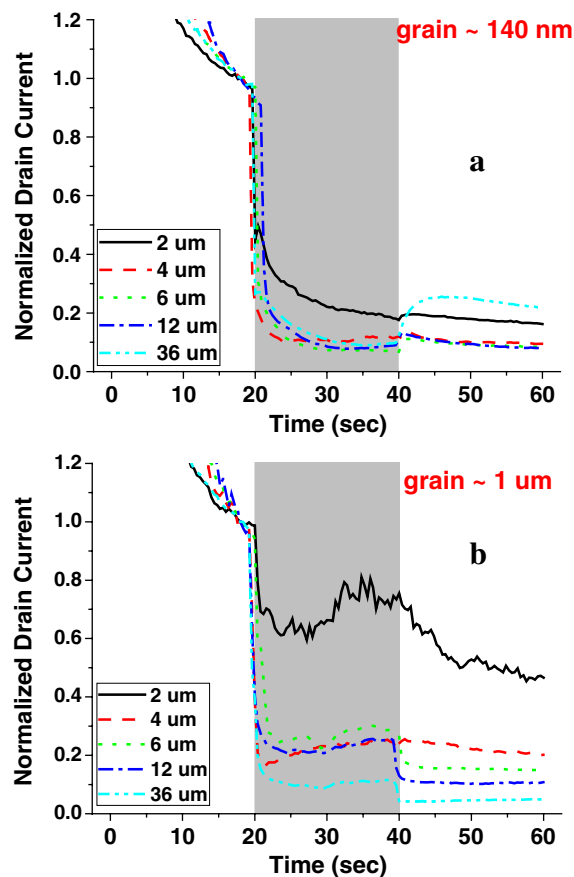


**Fig. 7** Sensing data of pentacene transistors on exposure to 1-pentanol: normalized  $I_{ds}$  under the conditions  $V_g=V_{ds}=-25$  V,  $v=45$  mL/min and  $d=2$  mm for different microscale channel lengths, with average pentacene grain size of 140 nm and 1 μm in **(a)** and **(b)** respectively. Reprinted with permission from Liang Wang, Daniel Fine, and Ananth Dodabalapur, Applied Physics Letters, 85, 6386 (2004). Copyright 2004, American Institute of Physics

on analyte delivery. The amplitudes of decreasing signals for 2 μm channels were smaller than those for longer channels. This effect is stronger with larger pentacene grains [Fig. 7(b)]. These results are consistent with reports of sensing effects dependent on organic grain sizes and channel lengths for the large scale [43, 44]. The sensing responses shown in Figs. 6 and 7 are reproducible for different devices with the same channel lengths and grain sizes, indicating that the response of pentacene transistors to the 1-pentanol vapor changes from decreasing  $I_{ds}$  to increasing  $I_{ds}$ , when the channel length shrinks from micron dimensions to 100 nm, with a crossover happening in a transition interval of channel length related to the grain sizes of pentacene.

#### Effect of analyte delivery

To examine the effect of analyte delivery on the sensing responses, we adjusted the analyte flux ( $v$ ) and the syringe nozzle–device distance ( $d$ ). It turns out that for all the

channel lengths and grain sizes, increasing  $v$  and decreasing  $d$  have similar effects, i.e., to increase the amplitude of the sensing signal. Also it was found that the sensing behavior was similar when operated in saturation region or linear region. Figure 8(a) gives an example of this sensing test on a 22 nm channel with an average grain size of 80 nm, measured under operation in the linear region. Figure 8(b) shows the SEM image of this device taken after sensing measurements.

#### Gate-voltage dependence of sensing responses

For micron-scale or larger channel lengths, the drain currents of P3HT transistors decreased in response to the analyte 1-pentanol, whereas an increase in current was observed for nanoscale channel lengths. Figures 9(a) and 9(b) show the two opposite responses at different gate voltages in 25  $\mu\text{m}$  and 15 nm channel-length devices, respectively. The currents are normalized to the pre-exposed base current measured just before the analyte was delivered. As seen from these figures, the gate modulation of the sensing effect is obvious in micron-scale channels. In

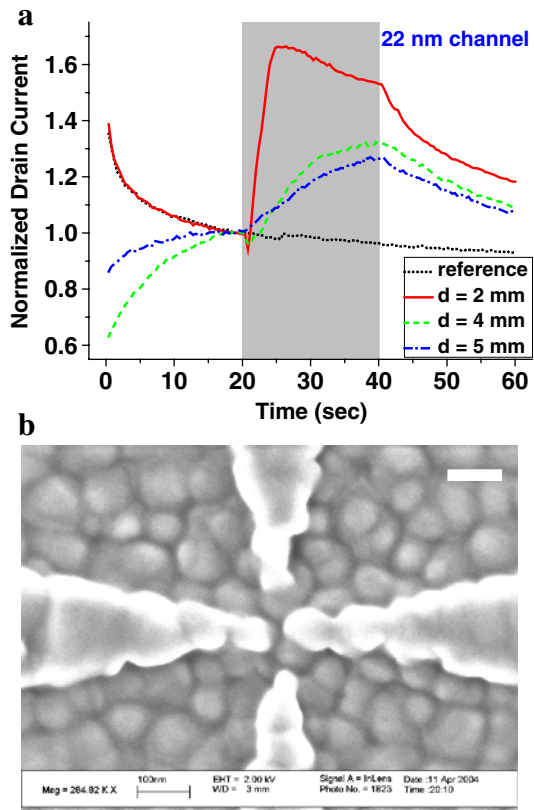


**Fig. 8** (a) Sensing data of a pentacene transistor of 22 nm channel in response to 1-pentanol, with  $V_g = -2$  V,  $V_{ds} = V_{side} = -0.4$  V and  $v = 45$  mL/min for different  $d$  (nozzle–device distance), “reference”=absence of analyte. (b) SEM image of the device in (a) taken after measurements, grain  $\sim 80$  nm, scale bar=100 nm. The appearing grains are pentacene. Reprinted with permission from Liang Wang, Daniel Fine, and Ananth Dodabalapur, Applied Physics Letters, 85, 6386 (2004). Copyright 2004, American Institute of Physics

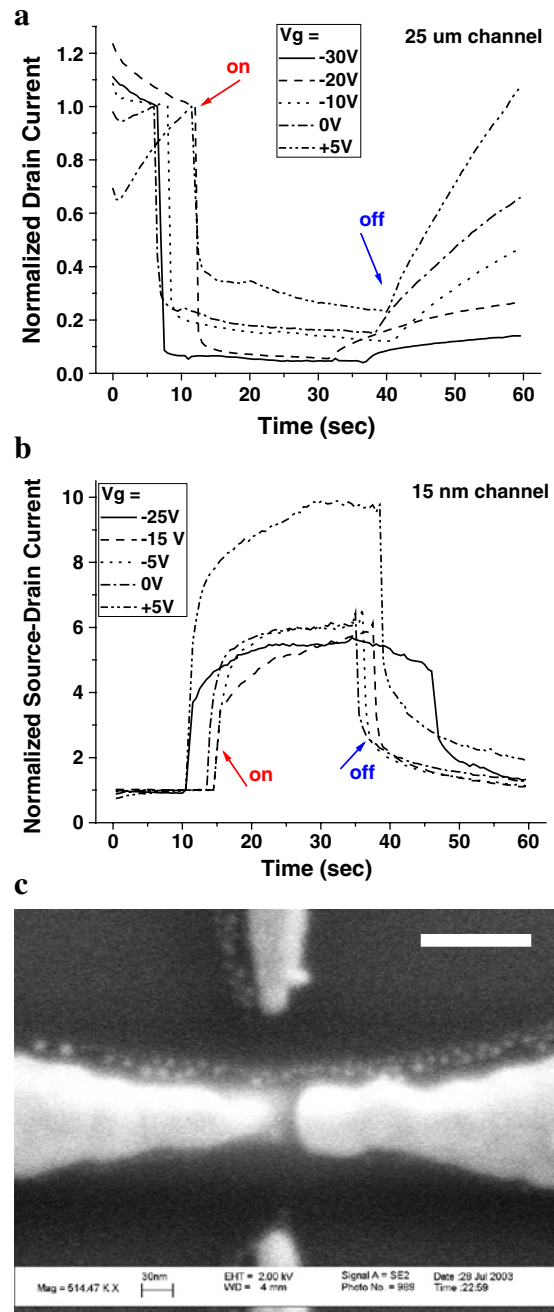


**Fig. 9** The sensing effects of P3HT transistors on exposure to 1-pentanol. (a) Sensing data of top-contact 25  $\mu\text{m}$  channel ( $W = 500$   $\mu\text{m}$ ) at different  $V_g$ , with  $V_{ds} = -30$  V. The drain current is normalized to that measured just before the analyte was delivered. (b) Sensing data of 15 nm channel at different  $V_g$ , with  $V_{ds} = V_{side} = -3$  V (two side guards were kept at the same potential as the drain). (c) SEM image of the device in (b), taken before depositing P3HT, scale bar=100 nm. Reprinted from Sens Actuators B (in press), Liang Wang, Daniel Fine, Saiful I Khondaker, Taeho Jung, Ananth Dodabalapur, Sub 10 nm conjugated polymer transistors for chemical sensing, Copyright (2005), with permission from Elsevier

nanoscale channels, the gate bias has less effect on the sensor response, possibly because of excess charges given by the analyte–semiconductor interaction which augment the gate-modulated charges, or reduction of the injection



barrier from the contacts to the semiconductor because of some kind of electrostatic analyte interaction at the contact surface. In addition, the dc  $I$ - $V$  characteristics of micron-scale channels recovered after reverse bias for 1 min whereas for nanoscale devices recovery was not complete, i.e. off-current increased and on/off ratio degraded even after reverse bias. Figure 9(c) shows the SEM image of the 15 nm channel taken before depositing P3HT.

#### Different type of analyte molecule

P3HT transistors with a series of channel lengths in the sub-micron range were used to examine the sensing responses of the conjugated polymer on exposure to another type of analyte—vanillin. As shown in Fig. 10(a) for sub micron channels, a decreasing response, as drain current, was observed for the 215 nm or larger channels on delivery

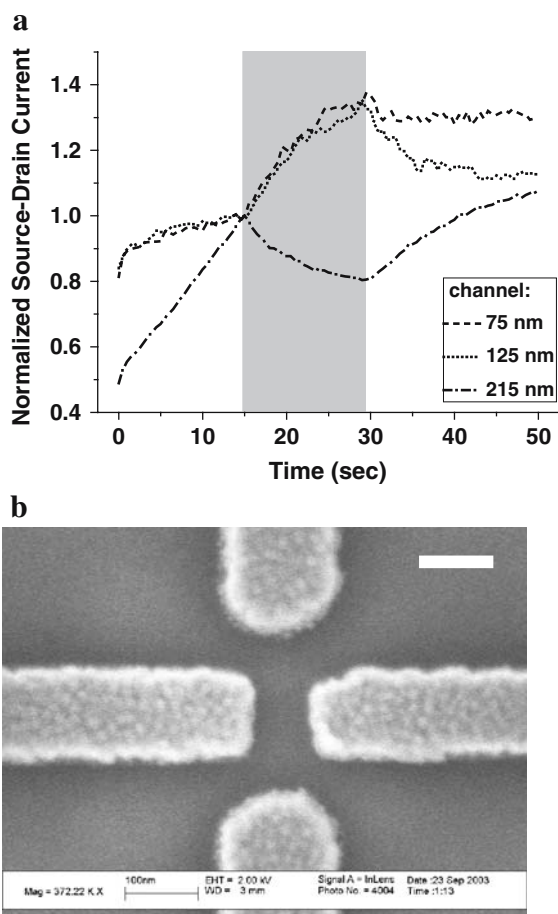


**Fig. 10** The sensing effects of P3HT transistors on exposure to vanillin. (a) Sensing data with  $V_g = -25$  V,  $V_{ds} = V_{side} = -10$  V and  $-15$  V for  $L < 100$  nm and  $L > 100$  nm respectively (two side guards were kept at the same potential as the drain), with different channel lengths and the same  $W/L$  of 3. (b) SEM image of a 75 nm channel taken before depositing P3HT, scale bar = 100 nm. Reprinted from Sens Actuators B (in press), Liang Wang, Daniel Fine, Saiful I Khondaker, Taeho Jung, Ananth Dodabalapur, Sub 10 nm conjugated polymer transistors for chemical sensing, Copyright (2005), with permission from Elsevier

of vanillin, whereas the 125 nm or smaller channels behaved in the opposite direction, i.e. an increase in current as the sensing response. The crossover of response behavior occurs in the interval of channel length 125–215 nm. Figure 10(b) shows the SEM image of a 75 nm channel taken before depositing P3HT. Based on the results for the sensing measurements of various channel lengths to the analytes 1-pentanol and vanillin, two factors are affecting sensor behavior, one causing a decrease in current (dominant in large  $L$  devices) and the other causing an increase (dominant in small  $L$  devices).

#### Discussion of the scaling behavior of sensing response

We discovered that when the device geometry was scaled down to nanoscale the sensing behavior was remarkably different from that of larger devices composed of the same materials for the same analyte. The direction and amplitude of sensing responses were found to be correlated with the channel length and the grain sizes of the organic semiconductor as sensing layer. These results follow the same trend as reported work for sensing effects dependent on channel lengths relative to grain sizes in large-scale organic transistors [43, 44]. These organic and conjugated polymer thin-film field-effect transistors have some features of similarity with polycrystalline oxide semiconductor sensors. In both, grain boundaries play a key role in large-scale devices and the analyte affects the electrical transport through grain boundaries and thereby modulates channel conductivity. According to a mobility study at low temperatures down to 77K, the transport mechanism of the transistors described in this paper was thermally activated hopping, which is mainly attributed to hopping at grain boundaries. Fig. 11 shows an Arrhenius plot of temperature-dependent mobility under different gate bias for a pentacene transistor with 2  $\mu$ m channel length. The plot follows the relationship for thermally activated hopping:  $\mu \approx \exp(-E_a/kT)$ . The activation energy  $E_a$  (energy barrier at

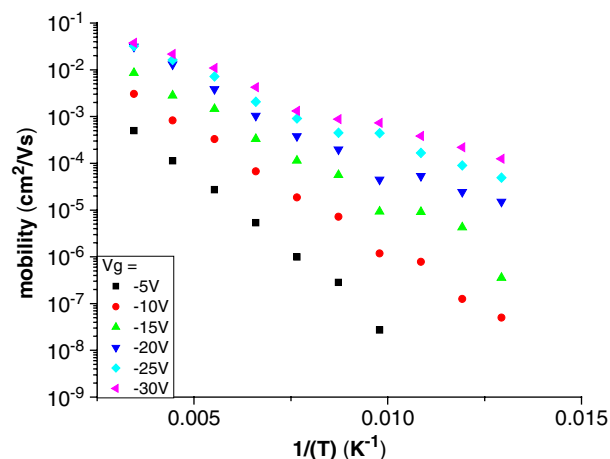


**Fig. 11** An Arrhenius plot of temperature-dependent mobility under different gate bias for a pentacene transistor with a 2  $\mu$ m channel length. Mobility values were calculated in the linear region of operation

a grain boundary) is 130 meV under  $-5V$  gate bias, and reduces to 52 meV under  $-30V$  gate bias. The mobility in the OTFTs presented in this work increases with increasing gate bias, as seen in Fig. 11, which is attributed to filling of the tail states of the density of states (DOS). Also, as Fig. 11 shows, the gate dependence is stronger at lower temperatures. These phenomena were well-known for disordered organic field-effect transistors where the band tail of localized states has a much wider distribution at grain boundaries than within each grain, because of the increased disorder at grain boundaries [61, 62]. It would be meaningful to investigate the effect of sensing action on the distribution of tail states by a combination of sensing experiments and temperature-dependent charge transport measurements. However this is practically difficult at this stage. Most volatile organic compounds (VOC) have a high vapor pressure, so the analytes will not remain at the sensing sites of device for very long. Therefore, comparison of temperature dependence of transistors before and after sensing might not give an accurate view of what happened during the sensing action. Furthermore, performing temperature-dependence experiments with the presence of analyte molecules is not feasible, because of the condensation effect of VOC under low temperatures.

For large-scale transistors, in which a number of grain boundaries are located within a channel, the analyte molecules at grain boundaries play a dominant role in the sensing response, where they trap the mobile charge carriers in the active channel and mainly result in a threshold shift of the transistor which leads to a decrease in drain current [15]. For devices with smaller dimensions there are fewer grain boundaries per channel so the effect of the decrease in drain current is reduced. When the channel length is close to or smaller than the average grain size, the dominant factor is reduction of the contact injection barrier by the analyte which leads to an increase in drain current. This is supported by sensing experiments conducted in our group for the same channel material with contact metals of different work functions [17]. Another possible cause of the increase of drain current as a sensing response observed in nanoscale OTFTs is a doping-like effect which could be the excess charges from the interaction between semiconductor grains and the analyte molecules. The overall sensing response is the result of a combination of these competing effects from different mechanisms—one causes decrease in drain current and the other causes increase, dominating at different length scales. It is indicative of scale being a very key element in the sensing process with organic transistor sensors.

#### Discussion of further research and potential applications

Organic/polymeric transistors and sensors have the flexibility to be improved for better performance and wider applications. Small receptor molecules could be easily incorporated into the semiconductor layer for higher selectivity and sensitivity [70–72]. Co-evaporating organic molecules and blending polymers can be used to make

composite films for a larger variety of detectable analytes. Most importantly, by combining novel technologies such as soft lithography [48, 73–78] and ink-jet printing [54, 79, 80], we might be able to fabricate chemical sensors based on nanoscale conjugated polymer transistors at fairly low cost. These sensors are also compatible with emerging low-cost organic electronic fabrication processes and can be integrated into processing/display electronics, also at low-cost.

One of the most attractive practical applications for organic and polymeric field-effect transistors is to make chemical sensors of high sensitivity and low cost. For this purpose, the following is important but remains to be accomplished:

- 1 To understand the interaction between analyte molecules and organic semiconductor layers. This will aid efforts to use experimental data to characterize the sensing events for pattern recognition of analytes.
- 2 By chemical and physical methods, to incorporate small receptor molecules into the organic semiconductor layer to enhance the sensitivity and selectivity of the nanoscale sensors. However, it is important to remember there is a trade-off between sensitivity and reversibility with respect to the binding strength between the analyte and any type of sensing layer. Careful study is necessary to find an optimum condition for different needs in different environments.
- 3 To investigate sensing responses for different analyte–semiconductor combinations to find an optimum material for a particular group of analytes. This will enable the building of a database of responses for a sensor array with the purpose of on-line analysis of the composition and concentration of a gas mixture, namely an electronic nose.
- 4 To investigate the effects of nanoscale morphology of the organic semiconductor layer on sensing behavior to find an optimum semiconductor morphology and device geometry for high sensitivity.
- 5 To improve the stability of the organic semiconductor in air. Many reports describe the effect of humidity on sensing performance and the sensor drift caused by the oxidation of organic materials over time. Therefore material science and encapsulation/package techniques are needed to overcome these problems.

---

#### Other types of nanoscale chemical and biological sensors

The inorganic material  $\text{LaFeO}_3$  has been made into a nanocrystalline thin-film sensing layer which acts as the gate of an ordinary n-channel metal oxide semiconductor field-effect transistor, to detect alcohol type analytes with good sensitivity and selectivity [63]. This type of sensor utilizes the wealth of grain boundaries and high surface area in the film to enhance the sensitivity. Also, nanocrystals and metal nanoparticles have been used with optical methods to detect biological binding events [64].

Because of the advantage of miniaturization and integration, however, electrical detection techniques are increasingly in demand. Functionalized carbon nanotubes and semiconductor nanowires have been used for electrical detection of chemical interactions and biological binding events [65–67]. Because of their quasi-one dimensional nature, nanotube and nanowire devices are very sensitive to small perturbations such as a change in conformation or charge state [64]. With their small diameters and high surface-to-volume ratios, nanowire and nanotube devices have potential in the manufacture of sensors of small size with low power dissipation levels and high sensitivity. In particular, a nanoelectrode array, based on vertically aligned multi-walled carbon nanotubes, with enough stability and repeatability for real commercialization has recently been developed [68]. Recently silicon nanowire field-effect transistors have been used for selective detection of the binding and unbinding event of a single virus to an antibody-modified nanowire by monitoring the change in conductance of the device [69].

**Acknowledgements** The authors would like to thank Dr Zhenan Bao (Stanford University, formerly Lucent) for providing some of the polythiophene and Professor Heinz von Seggern (Technical University of Darmstadt), Mr Taeho Jung, Mr Suvid Nadkarni, and Mr Debarshi Basu for helpful discussions. The authors would also like to thank NSF NIRT, DARPA, AFOSR, and Sematech AMRC for their financial support. Finally, we would like to thank the CNM and the TMI at the University of Texas at Austin for use of their facilities.

## References

- Gardner JW, Bartlett PN (1999) *Electronic noses: principles and applications*. Oxford University Press, Oxford
- Pearce TC, Schiffman SS, Nagle HT, Gardner JW (2003) (Eds), *Handbook of machine olfaction*, Wiley-VCH, Weinheim
- Ampuero S, Bosset JO (2003) *Sens Actuators B* 94:1
- Thaler ER, Kennedy DW, Hanson CW (2001) *Am. J Rhinol* 15:291
- Albert KJ, Lewis NS, Schauer CL, Sotzing GA, Stitzel SE, Vaid TP, Walt DR (2000) *Chem Rev* 100:2595
- Janata J (2003) *Proc IEEE*, 91(6):864–869
- Vincenzi D, Butturi MA, Guidi V, Carotta MC, Martinelli G, Guarnieri V, Brida S, Margesin B, Giacomozzi F, Zen M (2001) *Sens Actuators B* 77:95
- Ballantine DS, White RM, Martin SJ, Ricco AJ, Zellers, ET, Frye G, Wohltjen H (1997) *Acoustic wave sensors: theory, design, and physicochemical applications*, Academic Press, Boston, MA
- Cioffi N, Farella I, Torsi L, Valentini A, Sabbatini L, Zambonin PG (2003) *Sens Actuators B* 93:181–186
- Tyler McQuade D, Pullen Anthony E, Swager Timothy M (2000) *Chem Rev* 100:2537–2574
- Wollenstein J, Plaza JA, Cane C, Min Y, Bottner H, Tuller HL (2003) *Sens Actuators B* 93:350
- Haranyi G (1995) *Polymer films in sensor applications*. Technomic Publishing, Lancaster, PA, p. 58. Eggins BR (1996) *Biosensors: an introduction*. Wiley
- Burgmair M, Zimmer M, Eisele I (2003) *Sens Actuators B* 93:271–275
- Torsi L, Dodabalapur A, Sabbatini L, Zambonin PG (2000) *Sens Actuators B* 67:312–316
- Crone B, Dodabalapur A, Gelperin A, Torsi L, Katz HE, Lovinger AJ, Bao Z (2001) *Appl Phys Lett* 78(15):2229
- Crone BK, Dodabalapur A, Sarpeshkar R, Gelperin A, Katz HE, Bao Z (2002) *J Appl Phys* 91(12):10140
- Deepak Sharma and Ananth Dodabalapur, unpublished result
- Shirakawa H, Louis E, MacDiarmid AG, Chiang CK, Heeger AJ (1977) *J Chem Soc Chem Commun* 16:578
- Mitzi DB, Chondroudis K, Kagan CR (2001) *IBM J Res and Dev* 45(1):29–45
- Dimitrakopoulos CD, Mascaro DJ (2001) *J Res and Dev* 45(1):11
- Sheats James R (2004) *J Mater Res* 19(7):1974–1989
- Kelley TW, Baude PF, Gerlach C, Ender DE, Muyres D, Haase MA, Vogel DE, Theiss SD (2004) *Chem Mater* 16:4413–4422
- Koezuka H, Tsumura A, Ando T (1987) *Synth Met* 18:699
- Bredas JL, Calbert JP, da Silva Filho DA, Cornil J (2002) *PNAS* 99(9):5804–5809
- Kiguchi M, Nakayama M, Shimada T, Saiki K (2005) *Phys Rev B* 71(3) Art. No. 035332
- Dodabalapur A, Torsi L, Katz HE (1995) *Science*, 268(5208):270–271
- Dimitrakopoulos CD, Malenfant, PRL (2002) *Adv Mater* 14:99
- Sun YM, Liu YQ, Zhu DB (2005) *J Mater Chem*, 15(1):53–65
- Klauk H, Halik M, Zschieschang U, Schmid G, Radlik W, Weber W (2002) *J Appl Phys* 92(9):5259
- Gundlach DJ, Kuo C-C, Nelson SF, Jackson (1999) *TN 57th Annual Device Research Conference*, 164–165
- Bao Z, Dodabalapur A, Lovinger AJ (1996) *J Appl Phys Lett* 69(26):4108
- Sirringhaus H, Tessler N, Friend RH (1998) *Science* 280:1741
- Krumm J, Eckert E, Glauert WH, Andreas Ullmann, Walter Fix, and Wolfgang Clemens, *IEEE Electron Device Letters* 25(6):399
- Wingbrant H, Lundstrom I, Lloyd Spetz A (2003) *Sens Actuators B* 93:286–294
- Briand D, Wingbrant H, Sundgren H, van der Schoot B, Ekedahl L-G, Lundstrom I, de Rooij NF (2003) *Sens Actuators B* 93:276–285
- Tuller HL, Mlcak R (1998) *Curr. Opin. Solid State Mat Sci* 3:501
- Paulsson NJP, Winquist F (1999) *Forensic Sci Int* 105:95
- Janata J, Josowicz M (2003) *Nature Materials* 2:19
- Torsi L, Cioffi N, Di Franco C, Sabbatini L, Zambonin PG, Bleve-Zacheo T (2001) *Solid-State Electronics*, 45:1479
- Torsi L, Tanese MC, Cioffi N, Gallazzi MC, Sabbatini L, Zambonin PG (2004) *Sens Actuators B*, 98:204
- Torsi L, Taifuri A, Cioffi N, Gallazzi MC, Sassella A, Sabbatini L, Zambonin PG (2003) *Sens Actuators B*, 93:257
- Torsi L, Tanese MC, Cioffi N, Gallazzi MC, Sabbatini L, Zambonin PG, Raos G, Meille SV, Giangregorio MM (2003) *J. Phys. Chem. B*, 107:7589
- Torsi L, Lovinger AJ, Crone B, Someya T, Dodabalapur A, Katz HE, Gelperin A (2002) *J Phys Chem B* 106:12563
- Someya T, Katz HE, Gelperin A, Lovinger AJ, Dodabalapur A (2002) *Appl Phys Lett* 81(16):3079
- Madou MJ, Cubicciotti R (2003) *Proc IEEE* 91(6):830
- Collet J, Tharaud O, Chapoton, A, Vuillaume D (2000) *Appl Phys Lett* 76(14):1941
- Pannemann Ch, Diekmann T, Hilleringmann U (2003) *Microelectron Eng* 67–68:845–852
- Zhang Y, Patta JR, Ambily S, Shen Y, Ralph DC, Malliaras GG (2003) *Adv Mater* 15(19):1632
- Liang W, Daniel F, Taeho J, Debarshi B, von Seggern H, Dodabalapur A (2004) *Appl Phys Lett* 85(10):1772
- Knipp D, Street RA, Völkel AR (2003) *Appl Phys Lett* 82(22):3907
- Zhu Z, Mason JT, Dieckmann R, Malliaras, GG (2002) *Appl Phys Lett* 81(24):4643
- Sirringhaus H, Brown PJ, Friend RH, Nielsen MM, Bechgaard K, Langeveld-Voss BMW, Spiering AJH, Janssen RAJ, Meijer EW, Herwig P, De Leeuw DM (1999) *Nature* 401(6754):685–688
- Sirringhaus H, Kawase T, Friend RH, Shimoda T, Inbasekaran M, Wu W, Woo EP (2000) *Science*, 290(5499):2123–2126

54. Ong BS, Wu Y, Liu P, Gardner S (2004) *J Am Chem Soc* 126 (11):3378
55. Khondaker SI, Yao Z (2002) *Appl Phys Lett* 81(24):4613
56. Wang L, Jung T, Fine D, Khondaker SI, Yao Z, von Seggern H, Dodabalapur A (2003) *Proc 3rd IEEE Conf Nanotechnology*, (2):577–580
57. Matters M, de Leeuw DM, Herwig PT, Brown AR (1999) *Synth Met*, 102:998
58. Gomes HL, Stallinga P, Dinelli F, Murgia M, Biscarini F, de Leeuw DM, Muck T, Geurts J, Molenkamp LW, Wagner V (2004) *Appl Phys Lett* 84(16):3184
59. Horowitz G, Hajlaoui R, Delannoy P (1995) *J Phys III*, 5:355–371
60. Street RA, Northrup JE, Salleo A (2005) *Phys Rev B* 71:165202
61. Pinalli R, Suman M, Dalcanale E (2004) *Eur J Org Chem* 3:451–462
62. Srivastava DN, Shyam P (2004) *Proc Int Conf Electroanalytical Chemistry and Allied Topics*, Dona Paula, Goa, January, pp. 422
63. Aouni F, Rouis A, Ben Ouada H, Mlika R, Dridi C, Lamartine R (2004) *Mater Sci Eng C* 24(4):491–495
64. Gates BD, Xu Q, Christopher LJ, Wolfe DB, Whitesides GM (2004) *Annu Rev Mater Res* (34):339–372
65. Hua F, Sun Y, Gaur A, Meitl MA, Bilhaut L, Rotkina L, Wang J, Geil P, Shim M, Rogers JA, Shim A (2004) *Nano Lett* 4 (12):2467
66. Zaumseil J, Someya T, Bao ZN, Loo YL, Cirelli R, Rogers JA (2003) *Appl Phys Lett* 82(5):793–795
67. Torres CMS, Zankovych S, Seekamp J, Kam AP, Cedeno CC, Hoffmann T, Ahopelto J, Reuther F, Pfeiffer K, Bleidiessel G, Gruetzner G, Maximov MV, Heidari B (2003) *Mater Sci Eng C* 23(1–2):23–31
68. Resnick Doug, Sreenivasan SV, Grant Willson C (2005) *Mater Today* 8(2):34
69. Rogers JA, Bao Z, Baldwin K, Dodabalapur A, Crone B, Raju VR, Kuck V, Katz H, Amundson K, Ewing J, Drzaic P (2001) *PNAS* 98(9):4835–4840
70. de Gans BJ, Duineveld PC, Schubert, US (2004) *Advanced Materials*, 16(3):203–213
71. de Gans BJ, Schubert US (2004) *Langmuir* 20(18):7789–7793
72. Sirringhaus H, Shimoda T (2003) *MRS Bulletin* 28(11):802–803
73. Paul KE, Wong WS, Ready SE, Street RA (2003) *Appl Phys Lett* 83(10):2070
74. Zhao SQ, Sin JKO, Xu BK, Zhao MY, Peng ZY, Cai H (2000) *Sens Actuators B* 64 (1–3):83–87
75. Alivisatos P (2004) *Nature Biotechnol* 22(1):47
76. Collins PG, Bradley K, Ishigami M, Zettl A (2000) *Science* 287:1801
77. Kong J, Franklin NR, Zhou C, Chapline MG, Peng S, Cho K, Dai H (2000) *Science*, 287:622
78. Cui Y, Wei QQ, Park HK, Lieber CM (2001) *Science*, 293:1289
79. Li J, Ng HT, Cassell A, Fan W, Chen H, Ye Q, Koehne J, Han J, Meyyappan M (2003) *Nano Lett* 3(5):597
80. Patolsky F, Zheng G, Hayden O, Lakadamyali M, Zhuang X, Lieber CM (2004) *PNAS* 101(39):14017–14022